

EDGE-BASED SMOOTHED POINT INTERPOLATION METHODS

G. R. LIU^{*,†} and G. Y. ZHANG^{†,‡}

**Centre for Advanced Computations in Engineering Science
 Department of Mechanical Engineering
 National University of Singapore
 9 Engineering Drive 3, 117576, Singapore*

*†Singapore–MIT Alliance, E4-04-10
 4 Engineering Drive 3, 117576, Singapore*

‡smazg@nus.edu.sg

Received 9 September 2008

Accepted 10 October 2008

This paper formulates an edge-based smoothed point interpolation method (ES-PIM) for solid mechanics using three-node triangular meshes. In the ES-PIM, displacement fields are constructed using the point interpolation method (polynomial PIM or radial PIM), and hence the shape functions possess the Kronecker delta property, facilitates the enforcement of Dirichlet boundary conditions. Strains are obtained through smoothing operation over each smoothing domain associated with edges of the triangular background cells. The generalized smoothed Galerkin weak form is then used to create the discretized system equations and the formation is weakened weak formulation. Four schemes of selecting nodes for interpolation using the PIM have been introduced in detail and ES-PIM models using these four schemes have been developed. Numerical studies have demonstrated that the ES-PIM possesses the following good properties: (1) the ES-PIM models have a close-to-exact stiffness, which is much softer than for the overly-stiff FEM model and much stiffer than for the overly-soft node-based smoothed point interpolation method (NS-PIM) model; (2) results of ES-PIMs are generally of superconvergence and “ultra-accurate”; (3) no additional degrees of freedom are introduced, the implementation of the method is straightforward, and the method can achieve much better efficiency than the FEM using the same set of triangular meshes.

Keywords: Meshfree method; point interpolation method (PIM); finite element method (FEM); weakened weak form (W^2); edge-based strain smoothing.

1. Introduction

The finite element method (FEM) is one of the most powerful numerical methods and has been fully developed with many commercial software packages available [Zienkiewicz and Taylor (2000); Liu and Quek (2003)]. In application of the FEM

[‡]Corresponding author.

to practical and complicated engineering problems, triangular elements are preferred by the analysts as they can always be generated efficiently and automatically without manual operation for complicated problem domains. However, the FEM using linear triangular elements generally gives poor solutions, especially for stress components. This is because of the well-known *overly-stiff* phenomenon of a fully compatible FEM model of assumed displacement based on the standard Galerkin weak form.

Many efforts have been made to solve the overly-stiff problem of a compatible FEM model, such as the development of hybrid FEM formulations [Pian and Wu (2006)]. By introducing the generalized gradient smoothing technique into the schemes of meshfree methods and the FEMs, Liu and coworkers have developed a class of novel numerical methods that can effectively soften the model and result in a number of excellent properties, such as good accuracy, a high convergence rate, and even providing the upper bound solutions [Liu (2008a,b)]. Using shape functions generated by the point interpolation method (PIM), a node-based smoothed point interpolation method (NS-PIM or LC-PIM originally) has been developed for 2D problems [Liu *et al.* (2005)] and 3D problems [Zhang *et al.* (2007b)]. The theoretical foundation of the NS-PIM is the generalized smoothed Galerkin weak form with the generalized gradient smoothing techniques [Liu (2008a)] extended from the strain smoothing technique [Chen *et al.* (2001)]. Using the radial PIM shape functions and node-based strain smoothing operation, the node-based smoothed radial point interpolation method (NS-RPIM, or LC-RPIM originally) has also been formulated and applied for contact problems [Liu *et al.* (2006); Li *et al.* (2007)]. The PIM shape functions (with either polynomial or radial basis functions) possess the Kronecker delta property, which facilitates simple implementations of essential boundary conditions [Liu (2002)]. Using the same set of triangular elements, the NS-PIM and NS-RPIM can generally obtain more accurate and higher convergence solutions than the FEM and, more importantly, they can provide upper bound solutions in the energy norm for the force driven elasticity problems with homogeneous essential boundary conditions [Liu (2008); Zhang *et al.* (2007a); Zhang *et al.* (2008)]. Applying the strain smoothing operation to the finite elements leads to the smoothed finite element method (SFEM) [Liu, Dai and Nguyen (2007)] and the node-based smoothed finite element method (NS-FEM) [Liu and Nguyen *et al.* (2007)]. In the scheme of the SFEM, the cell-based smoothing domains are created over the elements (quadrilateral or n -sided polygonal), and each element can be further divided into a number of smoothing cells [Liu and Nguyen *et al.* (2007); Dai and Liu (2007)]. For the NS-FEM, the strain smoothing is performed over the smoothing domains associated with field nodes, and the method can be applied to triangular, four-node quadrilateral and n -sided polygonal elements. When using triangular elements, the NS-FEM is exactly the same as the NS-PIM using linear shape functions. As the NS-PIM behaves are overly-soft, leading to temporal instability in solving dynamic problems, the edge-based smoothed finite element method (ES-FEM) was formulated for both 2D and 3D problems [Liu, Nguyen

and Lam (2008); Nguyen *et al.* (2008)]. In the ES-FEM, the strain smoothing is performed over domains associated with each edge of triangular background cells. Compared with the node-based smoothing operation, the edge-based strain smoothing can properly reduce the softening effects and causes the ES-FEM model to have close-to-exact stiffness. The ES-FEM can provide more accurate results and eliminate the spurious nonzero energy modes, and hence works well for both static and dynamic problems.

In examining the above-mentioned works, Liu has established a weakened weak (W^2) formulation using the generalized gradient smoothing technique to unify all the developed numerical methods [Liu (2008a,b)]. The W^2 formulation seeks solutions in the so-called G space, which includes both continuous and discontinuous functions. Thus, it works for both compatible and incompatible displacements in the framework of the FEM and meshfree methods. Using the generalized strain smoothing technique, we can obtain the generalized smoothed Galerkin weak form applicable to all the above-mentioned methods.

In this work, an ES-PIM is formulated using polynomial and/or radial PIM shape functions to construct displacement fields, and smoothing the strains within edge-based smoothing domains. Based on the triangular background cells four schemes of selecting nodes for creating PIM shape functions have been introduced in detail. ES-PIM models using these four schemes have been developed: the ES-PIM of the T3 scheme [ES-PIM(T3)], the ES-PIM of the T6/3 scheme [ES-PIM(T6/3)], the ES-RPIM of the T6 scheme [ES-RPIM(T6)] and the ES-RPIM of the T2L scheme [ES-RPIM(T2L)]. A number of numerical examples have been studied to investigate various properties of all the four models of the ES-PIM, including accuracy, convergence rates and efficiency.

2. Summary of Basic Equations

Consider a two-dimensional static elasticity problem defined in domain Ω bounded by Γ ($\Gamma = \Gamma_u + \Gamma_t$; $\Gamma_u \cap \Gamma_t = 0$) governed by the equations

$$\mathbf{L}_d^T \boldsymbol{\sigma} + \mathbf{b} = 0 \quad \text{in } \Omega, \quad (1)$$

where \mathbf{L}_d is a matrix of the differential operator defined as

$$\mathbf{L}_d \left(\frac{\partial}{\partial x}, \frac{\partial}{\partial y} \right) = \begin{bmatrix} \frac{\partial}{\partial x} & 0 \\ 0 & \frac{\partial}{\partial y} \\ \frac{\partial}{\partial y} & \frac{\partial}{\partial x} \end{bmatrix}. \quad (2)$$

$\boldsymbol{\sigma}^T = \{\sigma_{xx} \ \sigma_{yy} \ \tau_{xy}\}$ is the vector that collects stress components and $\mathbf{b}^T = \{b_x \ b_y\}$ is the body force vector. The stresses relate the strains via the constitutive equation or the generalized Hook law, as follows:

$$\boldsymbol{\sigma} = \mathbf{D}\boldsymbol{\varepsilon}, \quad (3)$$

in which \mathbf{D} is the matrix of material constants, which is defined as follows:

$$\mathbf{D} = \frac{E}{1-v^2} \begin{bmatrix} 1 & v & 0 \\ v & 1 & 0 \\ 0 & 0 & \frac{1-v}{2} \end{bmatrix} \quad (\text{plane stress}), \quad (4)$$

$$\mathbf{D} = \frac{E(1-v)}{(1+v)(1-2v)} \begin{bmatrix} 1 & \frac{v}{1-v} & 0 \\ \frac{v}{1-v} & 1 & 0 \\ 0 & 0 & \frac{1-2v}{2(1-v)} \end{bmatrix} \quad (\text{plane strain}),$$

where E is Young's modulus and v is Poisson's ratio.

In Eq. (3), $\varepsilon^T = \{\varepsilon_{xx} \ \varepsilon_{yy} \ 2\varepsilon_{xy}\}$ is the vector of strains that relates to the displacements by the compatibility equation

$$\varepsilon = \mathbf{L}_d \mathbf{u}, \quad (5)$$

where $\mathbf{u} = \{u_x \ u_y\}^T$ is the displacement vector. Strains obtained using Eq. (5) are generally called *compatible* strains, and are termed $\tilde{\varepsilon}$ in this work.

There are two types of boundary conditions: Dirichlet (or essential/displacement) boundary conditions and Neumann (or natural/stress) boundary conditions.

Dirichlet boundary conditions:

$$\mathbf{u} = \mathbf{u}_\Gamma \quad \text{on } \Gamma_u, \quad (6)$$

where \mathbf{u}_Γ is the vector of the prescribed displacements on the essential boundary Γ_u .

Neumann boundary conditions:

$$\mathbf{L}_n^T \boldsymbol{\sigma} = \mathbf{t}_\Gamma \quad \text{on } \Gamma_t, \quad (7)$$

where \mathbf{t}_Γ is the vector of the prescribed traction on the natural boundary Γ_t , and \mathbf{L}_n is the matrix of the unit outward normal, which can be expressed as

$$\mathbf{L}_n(n_x, n_y) = \begin{bmatrix} n_x & 0 \\ 0 & n_y \\ n_y & n_x \end{bmatrix}. \quad (8)$$

3. Formulations of the ES-PIM

3.1. Displacement field approximation using the PIM

As the name implies, the point interpolation method (PIM) obtains the approximation by letting the interpolation function pass through the function values at each scattered node within the local supporting domain. Details of the construction of PIM shape functions can be found in the meshfree book by Liu [2002] and we give only a very brief introduction here.

3.1.1. Polynomial PIM and radial PIM

Two types of PIMs have been developed using different basis functions: the polynomial PIM, using polynomial basis functions [Liu and Gu (2001)]; and the radial PIM (RPIM), using radial basis functions [Wang and Liu (2002)].

For the polynomial PIM, the formulations start with the following assumption:

$$u(\mathbf{x}) = \sum_{i=1}^n P_i(\mathbf{x})a_i = \mathbf{P}^T(\mathbf{x})\mathbf{a}, \quad (9)$$

where $u(\mathbf{x})$ is a field variable function defined in the Cartesian coordinate space $\mathbf{x}^T = \{x \ y\}$, $P_i(\mathbf{x})$ is the basis function of monomials which is usually built utilizing Pascal's triangles, a_i is the corresponding coefficient, and n is the number of nodes in the local support domain. The complete polynomial basis of orders 1 and 2 can be written as

$$\begin{aligned} \mathbf{P}^T(\mathbf{x}) &= \{1 \ x \ y\} \quad (\text{basis of complete first order}), \\ \mathbf{P}^T(\mathbf{x}) &= \{1 \ x \ y \ x^2 \ xy \ y^2\} \quad (\text{basis of complete second order}). \end{aligned} \quad (10)$$

For the radial PIM, using radial basis functions augmented with polynomials, the field function can be approximated as follows:

$$u(\mathbf{x}) = \sum_{i=1}^n R_i(\mathbf{x})a_i + \sum_{j=1}^m P_j(\mathbf{x})b_j = \mathbf{R}^T(\mathbf{x})\mathbf{a} + \mathbf{P}^T(\mathbf{x})\mathbf{b}, \quad (11)$$

where $R_i(\mathbf{x})$ and $P_j(\mathbf{x})$ are radial basis functions and polynomial basis functions respectively, a_i and b_i are corresponding coefficients, n is the number of nodes in the local support domain and m is the number of polynomial terms. There are a number of different types of radial basis functions, and the Multiquadrics (MQ) is used in the present work with the augment of linear polynomials.

The coefficients in Eqs. (9) and (11) can be determined by enforcing the field function to be satisfied at the n nodes within the local support domain. Finally, the PIM shape functions can be obtained and the field function can be expressed as

$$u(\mathbf{x}) = \sum_{i=1}^n \varphi_i(\mathbf{x})d_i = \mathbf{\Phi}^T(\mathbf{x})\mathbf{d}, \quad (12)$$

where d_i is a nodal function value and $\varphi_i(\mathbf{x})$ is the PIM shape function (polynomial PIM or radial PIM) which possesses the Kronecker delta property [Liu and Gu (2005)]. In the above formulation, it is noticed that we need to properly select n nodes for interpolation, ensuring a nonsingular moment matrix [Liu (2002)].

3.1.2. T schemes for node selection

In the present work, the problem domain is first discretized with three-node triangular background cells which can always be generated efficiently and automatically without manual operation. The triangular meshes have been found to be most practical, robust, reliable and efficient for local support node selection [Liu and

Table 1. T-schemes.

Name	Nodes selection for interpolation at any point in a background cell	Application
T3 scheme	Three nodes of the home cell	Polynomial PIM
T6/3 scheme	For an interior home cell, three nodes of the home cell and three remote nodes of the three neighboring cells. For a boundary home cell, three nodes of the home cell.	Polynomial PIM Radial PIM
T6 scheme	For an interior home cell, three nodes of the home cell and three remote nodes of the three neighboring cells For a boundary home cell, three nodes of the home cell, two (or one) remote nodes of the neighboring cells and one (or two) field node which is nearest to the centroid of the home cell.	Radial PIM
T2L scheme	Nodes of the home cell plus one layer of nodes of the cells connected to the home element nodes (two layers of nodes are selected)	Radial PIM

Zhang *et al.* (2005); Kee *et al.* (2007)]. Thus, they are also used in this work. In theory, we require the inner angles of each triangular element to satisfy $0 < \theta < 180^\circ$, and, in practice, we require $15 < \theta < 120^\circ$, which can be easily met using a well-established triangulation algorithm such as the Delaunay algorithm. Triangular-cell-based node selection schemes are termed T schemes, and are listed in Table 1.

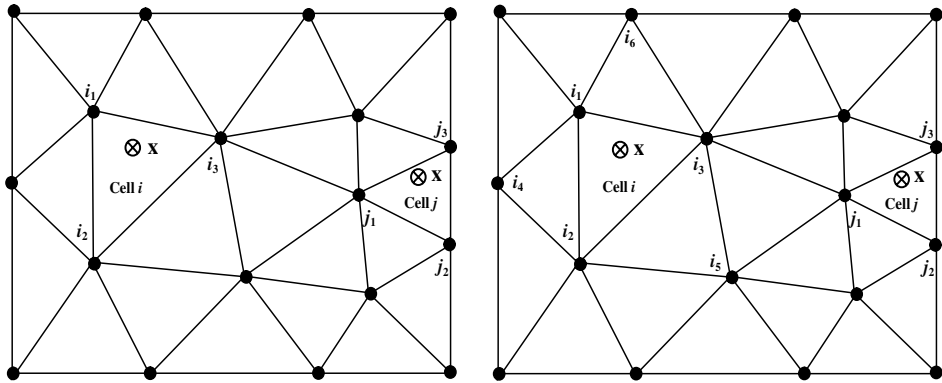
In the definition of types of T schemes, a *home cell* refers to the cell which holds the point of interest (usually the quadrature sampling point). An *interior home cell* is a home cell that has no edge on the boundary of the problem domain, and a *boundary home cell* is a home cell which has at least one edge on the boundary. Neighboring cells of an cell refer to the cells which share one edge with this cell. Details of the four types of T schemes are as follows:

T3 scheme

In the T3 scheme, we simply select three nodes of the home cell of the point of interest. As illustrated in Fig. 1(a), whether the point of interest (\mathbf{x}) is located in an interior cell (element i) or a boundary cell (element j), only the three nodes of the home cell (i_1-i_3 or j_1-j_3) are selected. The T3 scheme is used only for creating linear PIM shape functions by using polynomial basis functions. Note that the linear PIM shape functions so constructed are exactly the same as those in the FEM using linear triangular cells. The shape functions can always be constructed (the moment matrix will never be singular).

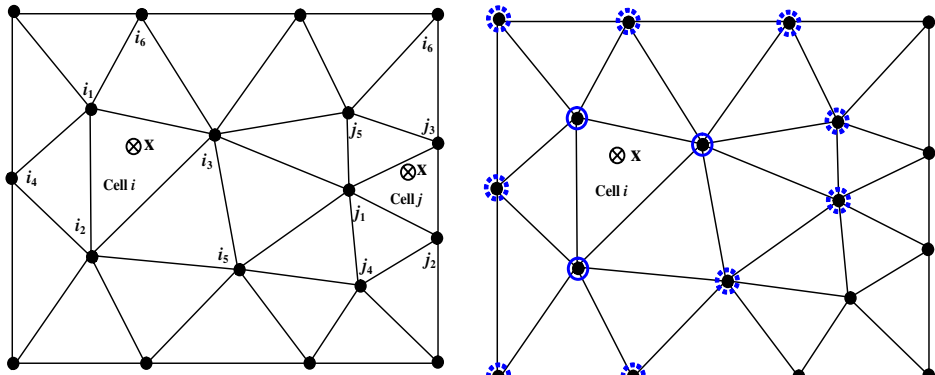
T6/3 scheme

The T6/3 scheme selects six nodes to interpolate a point of interest located in an interior cell and three nodes for those located in boundary cells. As illustrated in



(a) Illustration of the T3 scheme of node selection.

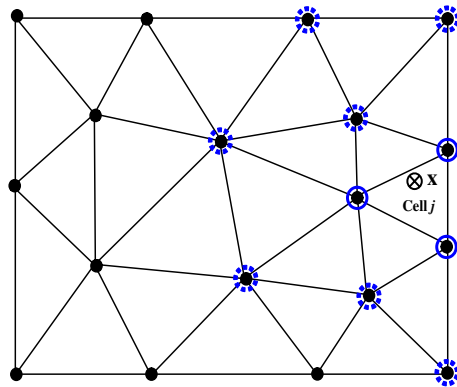
(b) Illustration of the T6/3 scheme of node selection.



○ First layer of nodes ⊗ Second layer of nodes

(c) Illustration of the T6 scheme of node selection.

(d) Illustration of the T2L scheme of node selection for the interior element.



○ First layer of nodes ⊗ Second layer of nodes

(e) Illustration of the T2L scheme of node selection for the boundary cell.

Fig. 1. Illustration of T schemes for support node selection based on three-node triangular cells.

Fig. 1(b), when the point of interest (\mathbf{x}) is located in an interior cell (cell i), we select six nodes: three nodes of the home cell (i_1-i_3) and another three nodes located at the remote vertices of the three neighboring cells (i_4-i_6). When the point of interest (\mathbf{x}) is located in a boundary cell (cell j), we select only three nodes of the home cell, i.e. j_1-j_3 .

The T6/3 scheme was devised for creating high-order PIM shape functions, where quadratic interpolations are performed for the interior cells and linear interpolations for the boundary cells. This scheme was first used in the NS-PIM [Liu *et al.* (2005)]. It not only successfully overcomes the singular problem which exists in the process of PIM approximation by using the polynomial basis but also improves the efficiency of the method. In addition, the use of three nodes for boundary cells insures passing the standard patch tests. Using the T6/3 scheme, the shape functions can always be constructed, as long as six such nodes can be found for all the interior cells.

T6 scheme

Same as the T6/3 scheme, the T6 scheme, shown in Fig. 1(c), selects six nodes for an interior home cell: three nodes of the home cell and three vertices at the remote vertices of the three neighboring cells (i_1-i_6 for cell i). However, for a boundary cell (cell j), the T6 scheme still selects six nodes: three nodes of the home cell (j_1-j_3), two remote nodes of the neighboring cells (j_4 and j_5) and one field node (j_6) which is nearest to the centroid of the home cell except for the five nodes that have been selected.

The T6 scheme was devised for constructing radial PIM shape functions, considering both accuracy and efficiency. Different from the T6/3 scheme, it selects six nodes for all home cells containing the point of interest. The shape functions can always be constructed because the radial moment matrix is always invertible for arbitrary scattered nodes so as to avoid using some specific shape parameters [Powell (1992)].

T2L scheme

The T2L scheme selects two layers of nodes to perform interpolation based on triangular meshes. As shown in Figs. 1(d) and 1(e), the first layer of nodes refers to the three nodes of the home cell, and the second layer contains those nodes which are directly connected to the three nodes of the first layer.

This scheme usually selects many more nodes than the T6 scheme, which leads to its being more time-consuming. The shape functions can always be constructed because the radial moment matrix is always invertible for arbitrary scattered nodes. We can use this scheme to create radial PIM shape functions with a high order of consistency and for extremely irregularly distributed nodes.

3.2. Edge-based smoothed strains

In the framework of W^2 formulation, the gradient of the field function (strains) will be obtained using the following generalized smoothing operation which considers

both continuous and discontinuous displacement functions [Liu (2008a,b)].

$$\widehat{\boldsymbol{\varepsilon}}_k = \begin{cases} \frac{1}{A_k} \int_{\Omega_k} \tilde{\boldsymbol{\varepsilon}}(\mathbf{x}) d\Omega = \frac{1}{A_k} \int_{\Gamma_k} \mathbf{L}_n \mathbf{u}(\mathbf{x}) d\Gamma, & \text{when } \mathbf{u}(\mathbf{x}) \text{ is continuous in } \Omega_k, \\ \frac{1}{A_k} \int_{\Gamma_k} \mathbf{L}_n \mathbf{u}(\mathbf{x}) d\Gamma, & \text{when } \mathbf{u}(\mathbf{x}) \text{ is discontinuous in } \Omega_k, \end{cases} \quad (13)$$

where $\tilde{\boldsymbol{\varepsilon}}$ is the compatible strain obtained using Eq. (5), $\widehat{\boldsymbol{\varepsilon}}_k$ is the smoothed strain over the smoothing domain (Ω_k), $A_k = \int_{\Omega_k} d\Omega$ is the area and Γ_k is the boundary of the smoothing domain Ω_k .

Note that the displacement fields in Eq. (13) can be continuous (T3 scheme) or discontinuous (all other T schemes). To perform the generalized strain smoothing, the problem domain is first discretized using three-node triangular background cells, and then the stationary and nonoverlapping smoothing domains are constructed based on these triangles such that $\Omega = \Omega_1 \cup \Omega_2 \cup \dots \cup \Omega_{N_s}$ and $\Omega_i \cap \Omega_j = \emptyset$, $i \neq j$, in which N_s is the number of smoothing domains. The rule is that we do not allow the boundary of Ω_i to share any finite parts of the discontinuous line segments for the assumed displacement field. In the framework of the ES-PIM, smoothing domains are constructed with respect to the edges of the triangular cells by connecting two ends of the edge to the centroids of two adjacent cells, as illustrated in Fig. 2. Thus, the number of smoothing domains (N_s) equals the number of edges of triangles (N_{edge}).

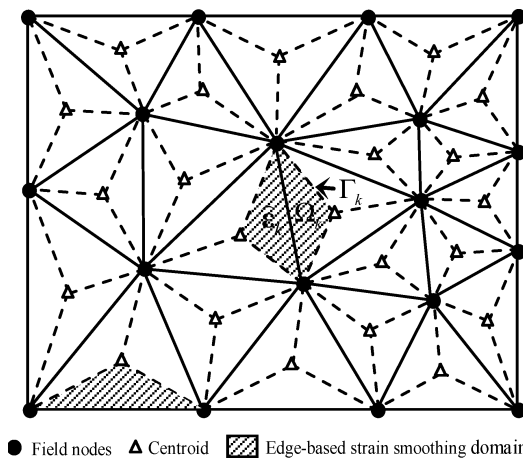


Fig. 2. Construction of edge-based strain smoothing domains, which are stationary, nonoverlapping and constructed based on the three-node triangular cells. For example, the strain smoothing domain corresponding to edge k , Ω_k , is formed by connecting two end points of edge k and two centroids of the adjacent triangular cells.

Substituting Eq. (5) into Eq. (13), the edge-based smoothed strain, $\widehat{\boldsymbol{\varepsilon}}_k$, can now be written in the following matrix form of nodal displacements:

$$\widehat{\boldsymbol{\varepsilon}}_k = \frac{1}{A_k} \int_{\Gamma_k} \mathbf{L}_n \boldsymbol{\Phi} \mathbf{d}_i d\Gamma = \sum_{i \in N_{\text{infl}}} \widehat{\mathbf{B}}_i(\mathbf{x}_k) \mathbf{d}_i, \quad (14)$$

where $\boldsymbol{\Phi}$ is the matrix of PIM shape functions and N_{infl} is the number of field nodes involved in constructing the smoothed strain fields within Ω_k . For example, when the T3 scheme is used and thus leads to linear displacement fields, N_{infl} equals exactly the number of nodes whose home cells are involved in the strain smoothing upon Ω_k . In Eq. (14), $\widehat{\mathbf{B}}_i(\mathbf{x}_k)$ is termed the *smoothed* strain matrix, which can be expressed as

$$\widehat{\mathbf{B}}_i(\mathbf{x}_k) = \begin{bmatrix} \widehat{\mathbf{b}}_{ix}(\mathbf{x}_k) & 0 \\ 0 & \widehat{\mathbf{b}}_{iy}(\mathbf{x}_k) \\ \widehat{\mathbf{b}}_{iy}(\mathbf{x}_k) & \widehat{\mathbf{b}}_{ix}(\mathbf{x}_k) \end{bmatrix}. \quad (15)$$

In the above equation, elements of the smoothed strain matrix are obtained as

$$\widehat{\mathbf{b}}_{il}(\mathbf{x}_k) = \frac{1}{A_k} \int_{\Gamma_k} \varphi_i(\mathbf{x}_k) n_l(\mathbf{x}_k) d\Gamma \quad (l = x, y). \quad (16)$$

Using the Gauss integration scheme, the above integration can be further expressed as follows:

$$\widehat{\mathbf{b}}_{il} = \frac{1}{A_k} \sum_{m=1}^{N_{\text{seg}}} \left[\sum_{n=1}^{N_{\text{Gauss}}} w_n \varphi_i(\mathbf{x}_{mn}) n_l(\mathbf{x}_m) \right] \quad (l = x, y) \quad (17)$$

where N_{seg} is the number of segments of the boundary Γ_k , N_{Gauss} is the number of the Gauss points located in each segment on Γ_k , and w_n is the corresponding weight number of the Gauss integration scheme. The value of N_{Gauss} should be determined according to the orders of shape functions.

3.3. Discretized system equations

For the present cases, the displacement field is not continuous except when using the polynomial PIM with the T3 scheme; we need to use the generalized smoothed Galerkin weak form or the weakened weak form [Liu (2008a,b)]:

$$\int_{\Omega} \delta(\widehat{\boldsymbol{\varepsilon}}(\mathbf{u}))^T \mathbf{D}(\widehat{\boldsymbol{\varepsilon}}(\mathbf{u})) d\Omega - \int_{\Omega} \delta \mathbf{u}^T \mathbf{b} d\Omega - \int_{\Gamma_t} \delta \mathbf{u}^T \mathbf{t}_{\Gamma} d\Gamma = 0, \quad (18)$$

which has exactly the same form as the standard Galerkin weak form. Thus, the formulation procedure is exactly the same as that in the standard FEM and all we need to do is to use the edge-based smoothed strain $\widehat{\boldsymbol{\varepsilon}}$ in place of the compatible strain fields $\boldsymbol{\varepsilon}$. The overall procedure of the presented methods is as follows. First, the

displacement field is constructed by using the PIM with different T schemes. Then, the smoothed strains $\widehat{\boldsymbol{\varepsilon}}$ is obtained using Eq. (13). Finally, by substituting the assumed displacements and the smoothed strains into the generalized Galerkin weak form [Eq. (18)], and invoking the arbitrary nature of the variation operations, a set of discretized algebraic system equations can be obtained in the matrix form

$$\widehat{\mathbf{K}}\mathbf{d} = \widehat{\mathbf{f}}, \quad (19)$$

where $\widehat{\mathbf{f}}$ is the force vector, which can be obtained as

$$\widehat{\mathbf{f}} = - \int_{\Omega} \boldsymbol{\Phi}^T \mathbf{b} d\Omega + \int_{\Gamma_t} \boldsymbol{\Phi}^T \mathbf{t}_{\Gamma} d\Gamma, \quad (20)$$

and the stiffness matrix $\widehat{\mathbf{K}}$ is assembled from the substiffness matrix for all the integration cells, which are exactly the edge-based smoothing domains for the present method:

$$\widehat{\mathbf{K}}_{ij} = \sum_{k=1}^{N_s} \widehat{\mathbf{K}}_{ij(k)}, \quad (21)$$

where $\widehat{\mathbf{K}}_{ij(k)}$ is the substiffness matrix associated with the integration cell k (i.e. smoothing domain Ω_k), which is computed using the smoothed strain matrix, as follows:

$$\widehat{\mathbf{K}}_{ij(k)} = \int_{\Omega_k} \widehat{\mathbf{B}}_i^T D \widehat{\mathbf{B}}_j d\Omega. \quad (22)$$

4. Numerical Implementation

4.1. ES-PIM models

According to the different types of PIM shape functions used (polynomial PIM or radial PIM) and the different T schemes adopted for selecting nodes, four ES-PIM models have been defined:

ES-PIM(T3)

In the framework of the ES-PIM(T3), a linear displacement field is constructed using polynomial PIM shape functions with the T3 scheme. Note that the ES-PIM(T3) is exactly the same as the ES-FEM using triangular mesh that was developed in the FEM setting. The displacement field in the ES-PIM(T3) is compatible.

ES-PIM(T6/3)

The ES-PIM(T6/3) is the ES-PIM where the displacement field is constructed using polynomial PIM shape functions with the T6/3 scheme. Thus, we can obtain quadratic displacement fields within the interior background cells and linear displacements on the boundary background cells. The displacement field in the ES-PIM(T6/3) is incompatible.

ES-RPIM(T6)

In the ES-RPIM(T6), we obtain the displacement fields within each triangular cell using the radial PIM shape functions with the T6 scheme. Compared to the following method using the T2L scheme, the ES-RPIM(T6) will save much more consulting time and effectively improve the efficiency of the method owing to using only six nodes for interpolation. The displacement field in the ES-PIM(T6) is incompatible.

ES-RPIM(T2L)

For the ES-RPIM(T2L), the displacement field within each triangular cell is obtained using radial PIM shape functions with the T2L scheme. Based on the triangular cells, the T2L scheme selects two layers of nodes and generally these nodes distribute evenly around the point of interest. However, as more nodes are involved in the interpolation, the ES-RPIM(T2L) is more expensive than other models. The displacement field in the ES-PIM(T2L) is incompatible.

4.2. Standard patch test

Passing the standard patch test requires that the displacements of all the interior nodes inside the patch follow “exactly” (to machine precision) the same linear function of the imposed displacement on the boundary of the patch. Numerically, passing the standard patch test can ensure a numerical method convergence to the exact solution [Zienkiewicz and Taylor (2000)].

A square patch discretized using 214 irregularly distributed nodes, as shown in Fig. 3, is studied using the present methods. The displacements are prescribed on all the boundaries by the following linear functions:

$$\begin{cases} u_x = 0.6x, \\ u_y = 0.6y. \end{cases} \quad (23)$$

The analytical solution for this patch test is a linear displacement field given by the above equation over the entire patch. The following error norm in displacements is used to examine the computed results:

$$e_d = \sqrt{\frac{\sum_{i=1}^{N_{\text{node}}} (u_i^{\text{exact}} - u_i^{\text{numerical}})^2}{\sum_{i=1}^{N_{\text{node}}} (u_i^{\text{exact}})^2}}, \quad (24)$$

where the superscript “exact” denotes the exact or analytical solution, the superscript “numerical” denotes a numerical solution obtained using a numerical method including the present ES-PIM, and N_{node} is the number of total field nodes.

Table 2 lists the displacement norm errors of numerical results for the standard patch test obtained using different models of the ES-PIM. All the four models can pass the patch test to machine accuracy and hence are capable of reproducing linear displacement fields “exactly.” Note that to impose the linear Dirichlet boundary

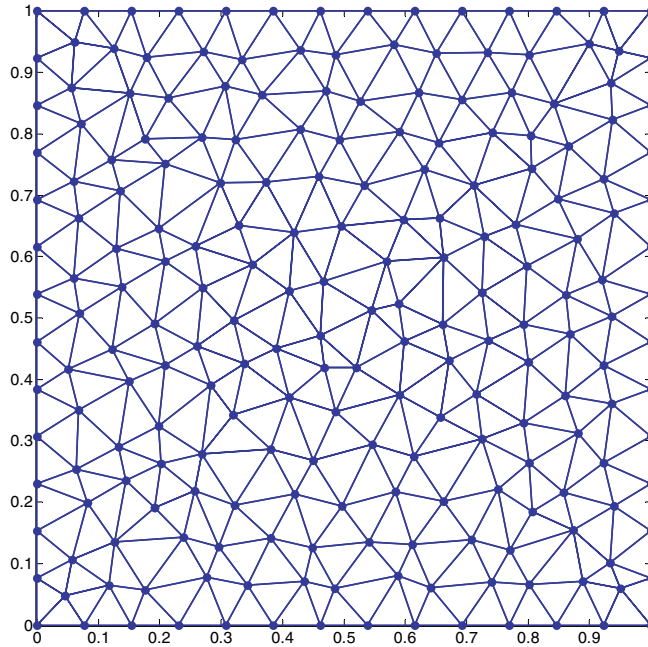


Fig. 3. Unique square patch discretized with 214 irregularly distributed nodes.

Table 2. Error norm in displacements of numerical results for the standard patch obtained using ES-PIMs.

ES-PIM models	Error in displacement norm
ES-PIM(T3) (compatible)	1.7690582E-15
ES-PIM(T6/3) (incompatible)	2.6089673E-14
ES-RPIM(T6) (incompatible)	1.6020897E-15
ES-RPIM(T2L) (incompatible)	2.1726750E-15

conditions exactly along the problem boundaries, linear interpolation should be used for the points of interest located on the boundaries.

5. Numerical Examples

Some numerical examples are studied to investigate the properties of ES-PIM models. The materials used are all linear elastic, with Young's modulus $E = 3.0 \times 10^7$ and Poisson's ratio $\nu = 0.3$. The units can be any consistent unit system.

5.1. Cantilever beam

A benchmark problem of the cantilever beam is studied which is of length L and height D , as shown in Fig. 4. The beam is subjected to a parabolic traction on its

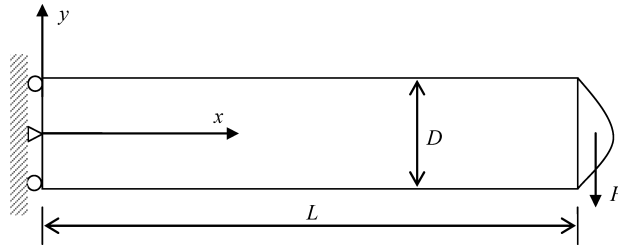


Fig. 4. Cantilever beam subjected to a parabolic traction on the right edge.

right edge. It is assumed to have unit thickness, and analytical solutions based on the plane stress theory are available [Timoshenko and Goodier (1970)]:

$$u_x = -\frac{py}{6EI} \left[(6L - 3x)x + (2 + \nu) \left(y^2 - \frac{D^2}{4} \right) \right], \quad (25)$$

$$u_y = \frac{p}{6EI} \left[3\nu y^2(L - x) + (4 + 5\nu) \frac{D^2 x}{4} + (3L - x)x^2 \right], \quad (26)$$

$$\sigma_x = -\frac{p(L - x)y}{I}, \quad \sigma_y = 0, \quad \sigma_{xy} = \frac{p}{2I} \left[\frac{D^2}{4} - y^2 \right], \quad (27)$$

where I is the moment of the inertia, given as $I = D^3/12$. The values of the parameters are taken as $L = 50$, $D = 10$ and $P = -1000$.

Using the same set of triangular meshes, the cantilever beam is studied using the presented ES-PIM models. Further, we study this problem using the FEM and NS-PIM(T3) with the same triangular meshes. The FEM can serve as the “bottom line”: any ES-PIM model that is established based on the smoothed bilinear form is softer than the standard FEM model, which is built based on the bilinear form. The NS-PIM is chosen for comparison, because we know that it gives upper bound solutions.

Figure 5 plots the convergence of the solutions in the displacement norm for the cantilever beam solved using different methods. The present ES-PIM models, together with the FEM and NS-PIM, converge with the reducing average nodal spacing (h) at about the same rate, which is close to the theoretical value of 2.0 for both the weak and weakened weak (W^2) formulations [Liu (2008b)]. In terms of accuracy, except for the NS-PIM using the T3 scheme, which obtains almost the same results as the FEM, the present four ES-PIM models obtain about-ten-times-more-accurate solutions than the FEM. Note that although the T2L scheme uses many more nodes than the T6 scheme, which uses only six nodes for interpolation, the results of these two schemes have similar accuracy and convergence rates.

Figure 6 plots the convergence of the solutions in the energy norm for the cantilever beam problem solved using different methods. The energy norm error

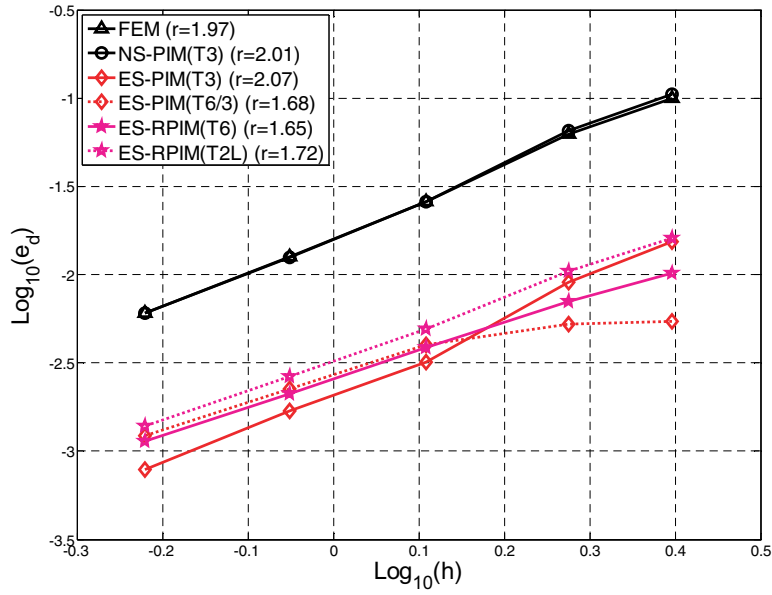


Fig. 5. Convergence of the numerical results in the displacement norm for the problem of the cantilever beam solved using different methods and the same set of irregular triangular meshes.

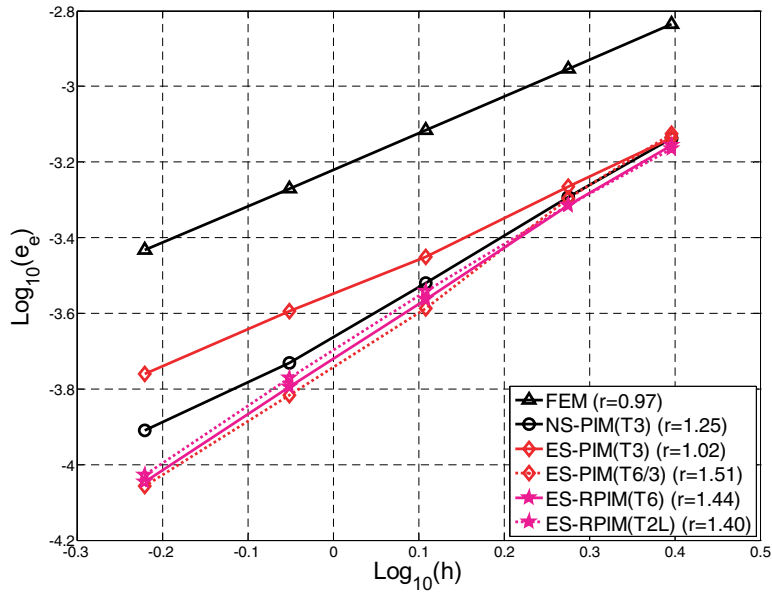


Fig. 6. Convergence of the numerical results in the energy norm for the problem of the cantilever beam solved using different methods and the same set of irregular triangular meshes.

indicator is defined as follows:

$$e_e = \frac{1}{A} \sqrt{\frac{1}{2} \int_{\Omega} (\boldsymbol{\varepsilon}^{\text{exact}} - \boldsymbol{\varepsilon}^{\text{numerical}})^T \mathbf{D} (\boldsymbol{\varepsilon}^{\text{exact}} - \boldsymbol{\varepsilon}^{\text{numerical}}) d\Omega}, \quad (28)$$

where A is the area of the problem domain. It can be found that the NS-PIM and the present ES-PIMs have better accuracy and converge faster than the FEM. We know that the theoretical convergence rate in the energy norm of the FEM based on the weak form is 1.0, and Liu has found that W^2 formulation can have a theoretical rate of 1.5 [Liu (2008b)]. For the case of the cantilever, the numerical convergence rate of the FEM is 0.97, which is a little less than the theoretical one for weak formulation. The convergence rates of all the methods based on W^2 formulation are between 1.0 and 1.5. In terms of both accuracy and convergence rate, the ES-PIM(T6/3) performs better than the ES-PIM(T3) and stands out together with the ES-RPIM of the T6 scheme and the T2L scheme.

By plotting the errors in displacement and energy norms against the computational cost (seconds), Figs. 7 and 8 show a comparison of efficiency between all the numerical methods studied. The results are obtained using full matrix solver. Except for the NS-PIM(T3), which performs a little worse in terms of the displacement error, all the models of the ES-PIM are more efficient than the FEM, with respect to both displacement and energy error norms. The ES-PIM(T3) and ES-PIM(T6/3) perform similarly to each other. For the two schemes of the ES-RPIM, although the T6 scheme uses fewer nodes than the T2L scheme, the former still obtains better efficiency than the latter. In terms of efficiency, two models of the ES-PIM stand out: the ES-PIM(T3)

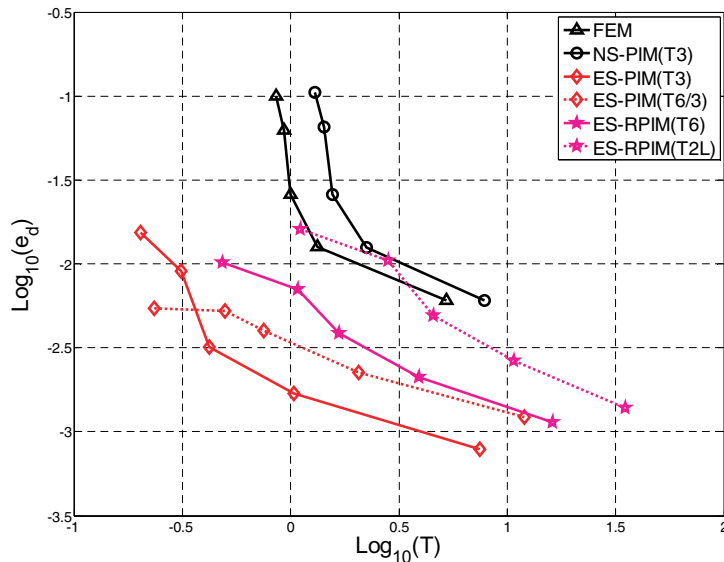


Fig. 7. Computational cost (seconds) vs. error in displacement norm. Comparison of efficiency between different methods via the problem of the cantilever beam.

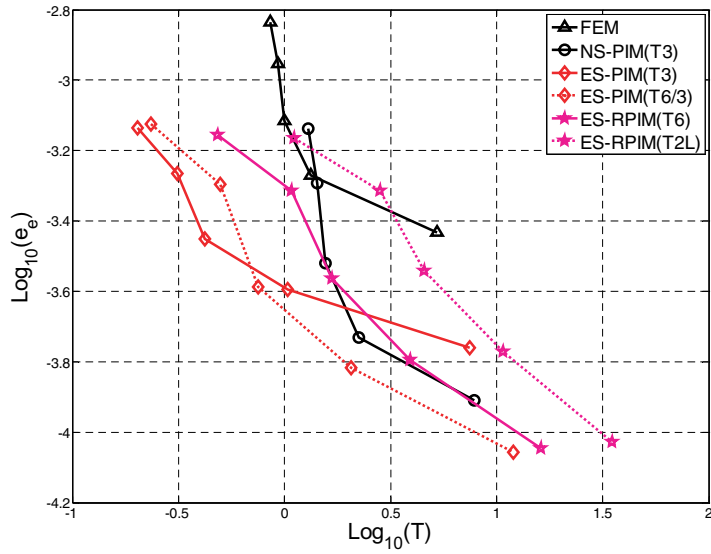


Fig. 8. Computational cost (seconds) vs. error in energy norm. Comparison of efficiency between different methods via the problem of the cantilever beam.

performed best in the displacement error norm, and the ES-PIM(T6/3) performed best in the energy error norm.

Figure 9 plots the process of strain energies converging to the exact solution for the cantilever using different methods. As expected, the FEM and NS-PIM give

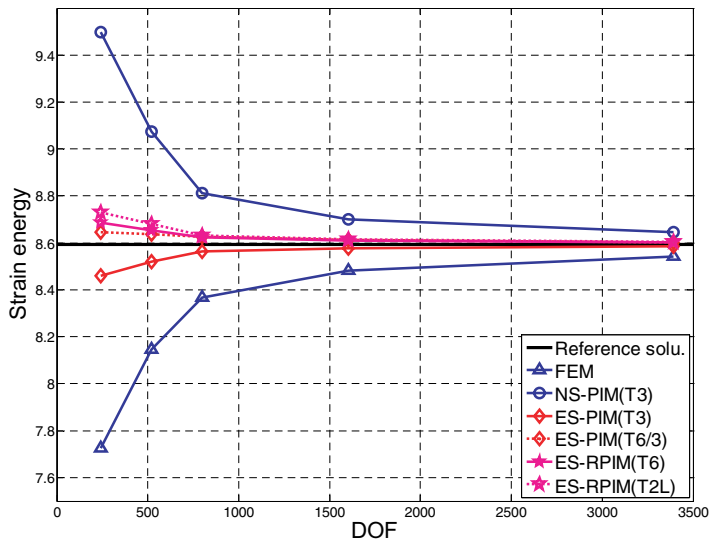


Fig. 9. Solutions (in the energy norm) converging to the exact solution for the problem of the cantilever beam obtained using different methods and the same set of irregular triangular meshes.

the lower and the upper bound respectively and also provide the energy bound to the four ES-PIM models. The ES-PIM of the T3 scheme performs more softly than the FEM but more stiffly than the NS-PIM, and gives a lower bound solution, which is the same as the performance of the ES-FEM using triangular elements [Liu, Nguyen and Lam (2008a)]. As we discussed previously [Liu and Zhang (2008)], one issue that affects the softness of the model is the order of shape functions used in the displacement approximation: when higher order shape functions are used, the displacements approximated in a smoothing domain are closer to the exact solution, which will reduce the stiffening effect and vice versa. Thus, we can find from Fig. 9 that the ES-PIM with the T6/3 scheme performs more softly than the ES-PIM of the T3 scheme. Between the two schemes of the ES-RPIM, as the T2L scheme uses more nodes than the T6 scheme for interpolation of displacements, the former performs more softly than the latter. This confirms our analysis of softening effects. Although the three models, i.e. the ES-PIM(T6/3), ES-RPIM(T6) and ES-RPIM(T2L), perform more softly than the ES-PIM(T3), it cannot be concluded that these three models can always obtain upper bound solutions, even if they did for this particular case. The following numerical results will also show this phenomenon.

5.2. Infinite plate with a circular hole

Another benchmark problem is studied, which is an infinite solid with a central circular hole ($a = 1$) and subjected to a unidirectional tensile ($T_x = 10$), as shown in Fig. 10. Due to the twofold symmetry, only one quarter is modeled with $b = 5$ and symmetry conditions are imposed on the left and bottom edges. The analytical solution is available for this problem [Timoshenko and Goodier (1970)]:

$$u_r = \frac{T_x}{4\mu} \left\{ r \left[\frac{\kappa - 1}{2} + \cos(2\theta) \right] + \frac{a^2}{r} [1 + (1 + \kappa) \cos(2\theta)] - \frac{a^4}{r^3} \cos(2\theta) \right\}, \quad (29)$$

$$u_\theta = \frac{T_x}{4\mu} \left[(1 - \kappa) \frac{a^2}{r} - r - \frac{a^4}{r^3} \right] \sin(2\theta), \quad (30)$$

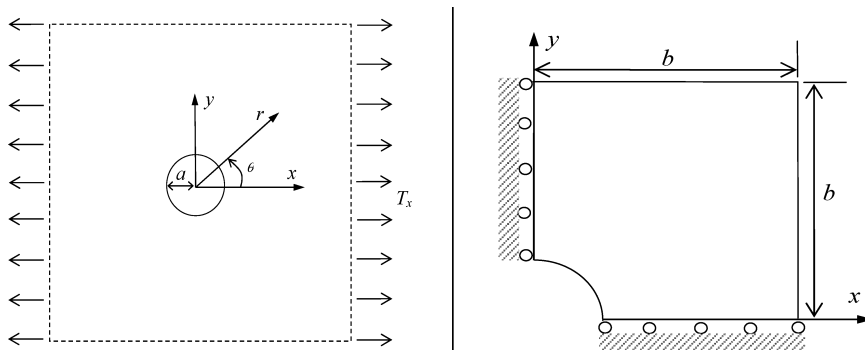


Fig. 10. Infinite solid with a circular hole subjected to uniform tensile and its quadrant model.

$$\sigma_{xx} = T_x \left\{ 1 - \frac{a^2}{r^2} \left[\frac{3}{2} \cos(2\theta) + \cos(4\theta) \right] + \frac{3a^4}{2r^4} \cos(4\theta) \right\}, \quad (31)$$

$$\sigma_{yy} = -T_x \left\{ \frac{a^2}{r^2} \left[\frac{1}{2} \cos(2\theta) - \cos(4\theta) \right] + \frac{3a^4}{2r^4} \cos(4\theta) \right\}, \quad (32)$$

$$\sigma_{xy} = -T_x \left\{ \frac{a^2}{r^2} \left[\frac{1}{2} \sin(2\theta) + \sin(4\theta) \right] - \frac{3a^4}{2r^4} \sin(4\theta) \right\}, \quad (33)$$

where

$$\mu = \frac{E}{2(1+\nu)}, \quad \kappa = \begin{cases} 3-4\nu & (\text{plane strain}), \\ \frac{3-\nu}{1+\nu} & (\text{plane stress}). \end{cases} \quad (34)$$

In the above equations, (r, θ) are the polar coordinates and θ is measured counterclockwise from the positive x axis. We studied the problem under plane stress conditions, and traction boundary conditions are imposed on the right and upper edges with the exact stresses obtained using Eqs. (31)–(33).

The convergence property in terms of displacement of all the methods is shown in Fig. 11. Except for the NS-PIM(T3), which obtains similar results to the FEM, all other ES-PIM models provide much more accurate and faster convergent solutions than the FEM. In detail, two schemes of the ES-PIM and ES-RPIM(T6) obtain similar results, and the ES-RPIM(T2L) stands out in terms of both accuracy and convergence rate. Figure 12 plots the convergence of the solutions in the energy

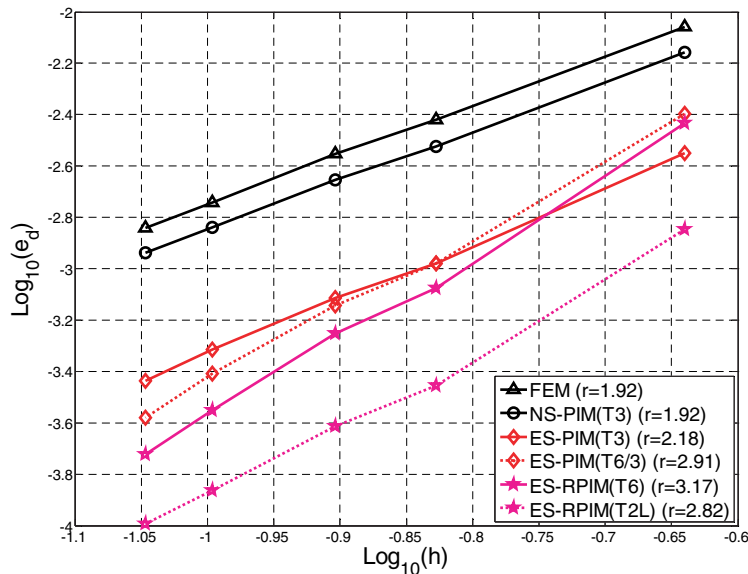


Fig. 11. Convergence of the numerical results in the displacement norm for the problem of the infinite solid with a hole solved using different methods and the same set of irregular triangular meshes.

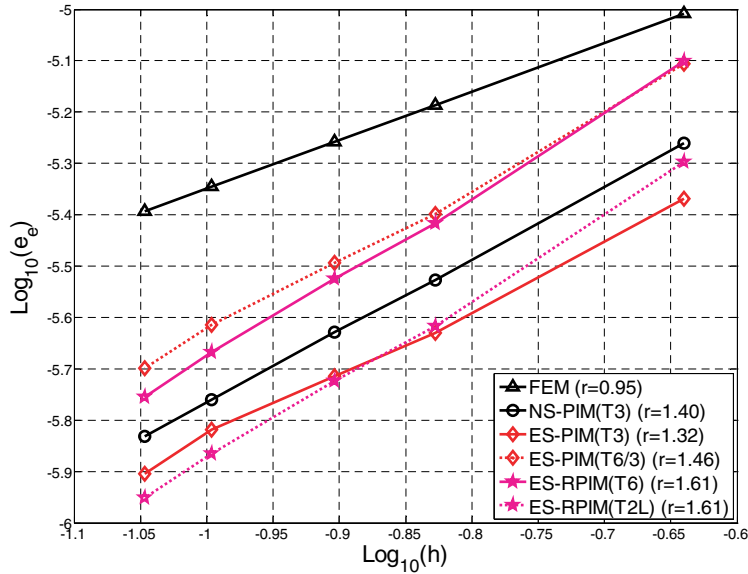


Fig. 12. Convergence of the numerical results in the energy norm for the problem of the infinite solid with a hole solved using different methods and the same set of irregular triangular meshes.

norm for different methods. Again, it can be found that the NS-PIM(T3) and four ES-PIM models all obtain much better results than the FEM, which are not only of higher accuracy but also achieve faster convergence rates.

Efficiencies of all the methods are illustrated in Figs. 13 and 14 by plotting the errors in displacement and energy norms against the computational cost. In terms of the displacement error, the NS-PIM(T3) performs a little worse than the FEM, but the former is much better than the latter with respect to the energy error. All the ES-PIM models show much higher efficiency than the FEM. Again, we found that the ES-RPIM of the T6 scheme and the T2L scheme obtain similar efficiency, although the latter uses more nodes for interpolation.

Figure 15 shows the process of strain energies converging to the exact one for the infinite solid with a hole problem solved using different methods. The FEM and NS-PIM provide lower and upper bound solutions respectively and they also bound the solutions of ES-PIM models from two sides. As we discussed previously, the ES-PIM of the T6/3 scheme performs more softly than the ES-PIM(T3) when the problem domain is discretized using “more” cells. For the T6/3 scheme, we use only six nodes for those interior elements and still use three nodes for boundary elements. When fewer cells are used, the ratio of the interior elements is not very high and the T6/3 scheme may perform even more stiffly than the T3 scheme. However, the ES-PIM of the T6/3 scheme will be softer than the model of the T3 scheme when we use “more” cells to discretize the problem domain. For the two schemes of the ES-RPIM, again the T2L scheme performs more softly than the T6 scheme for using

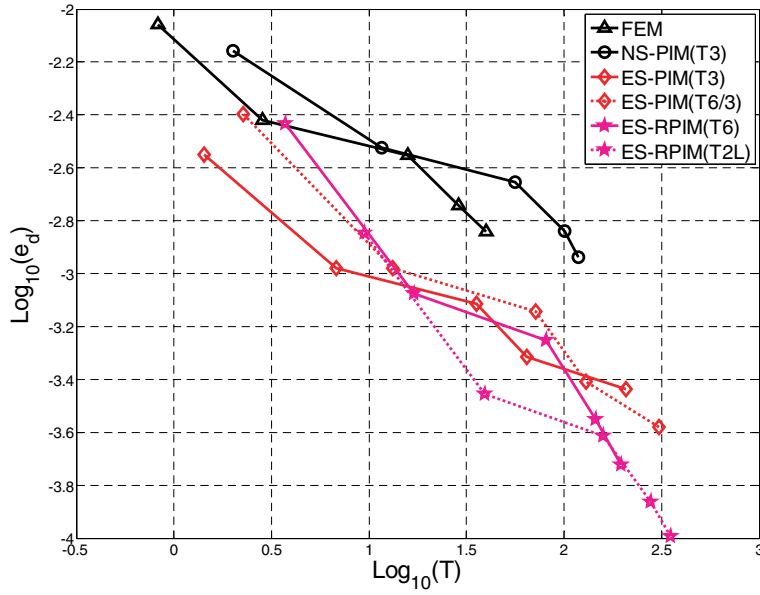


Fig. 13. Computational cost (seconds) vs. error in displacement norm. Comparison of efficiency between different methods via the problem of the infinite solid with a hole.

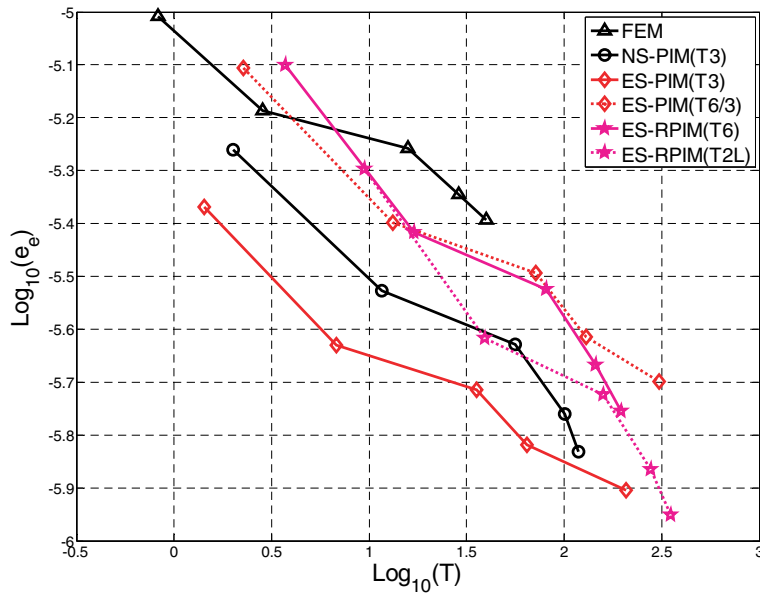


Fig. 14. Computational cost (seconds) vs. error in energy norm. Comparison of efficiency between different methods via the problem of the infinite solid with a hole.

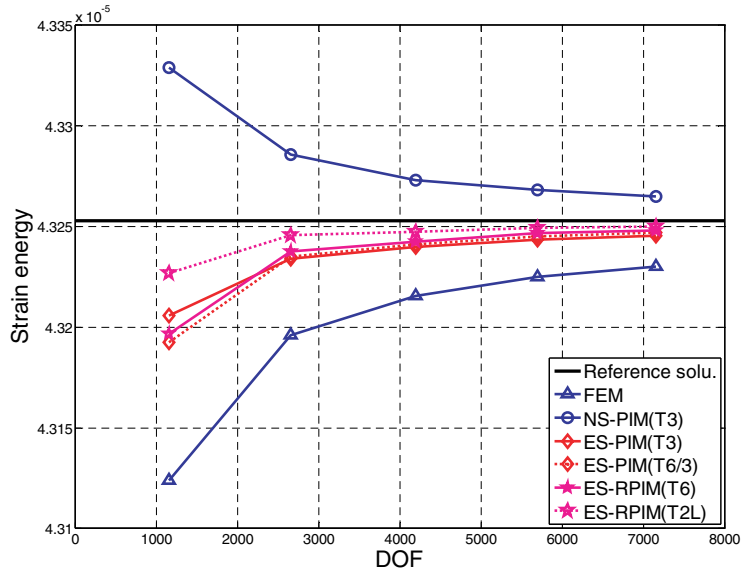


Fig. 15. Solutions (in the energy norm) converging to the exact solution for the problem of the infinite solid with a hole obtained using different methods and the same set of irregular triangular meshes.

more nodes for interpolation. All the ES-PIMs perform more softly than the FEM and provide lower bound solutions for this problem.

5.3. Automotive part: Rim

Finally, a typical rim of an automotive component is studied using the present method. As shown in Fig. 16, the rim is restricted along the inner circle and a

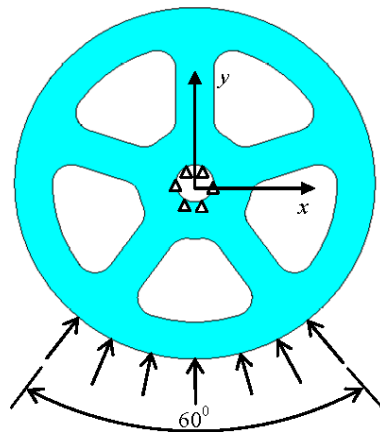


Fig. 16. Model of an automotive rim.

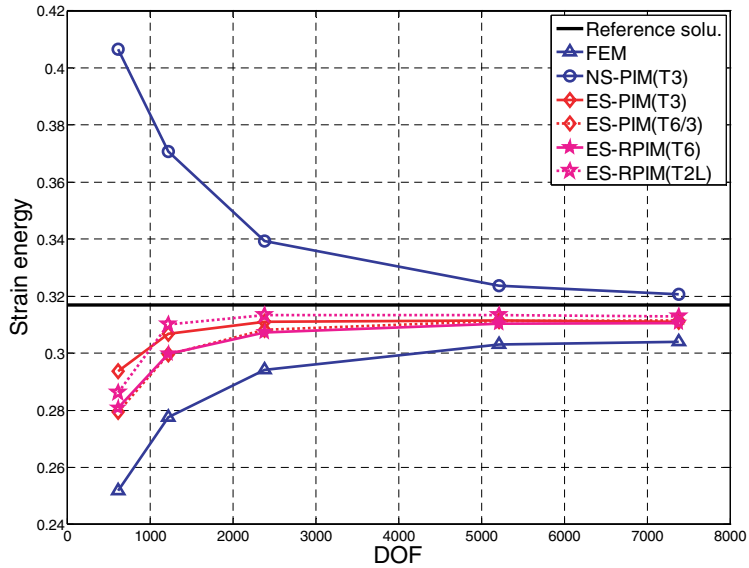


Fig. 17. Solutions (in the energy norm) converging to the exact solution for the problem of the rim obtained using different methods and the same set of irregular triangular meshes.

uniform pressure of 100 units is applied along the outer arc edge of 60° . The rim is studied as a plane stress problem using the FEM, NS-PIM and present ES-PIMs with the same set of triangular elements.

The process of strain energies converging to the reference one for the rim solved using different methods is plotted in Fig. 17. It can be found again that the FEM provides a lower bound, the NS-PIM provides an upper bound, and they also bound the solutions of ES-PIMs. For the ES-PIM with the T3 and T6/3 schemes, the former performs more softly when the problem domain is discretized using fewer cells; but the latter will be softer than the former when we use more cells. For the ES-RPIM of the T6 and T2L schemes, again we found that the latter performs more softly than the former, owing to using more nodes for interpolation.

6. Conclusions

In this work, edge-based smoothed point interpolation methods (ES-PIMs) have been proposed, in which the displacement fields are approximated using PIM shape functions (polynomial PIM or radial PIM) and the strains are smoothed over the edge-based smoothing domains. Four schemes for nodes selection of interpolation have been proposed based on triangular background cells and thus four ES-PIM models have been developed, i.e. ES-PIM(T3), ES-PIM(T6/3), ES-RPIM(T6) and ES-RPIM(T2L). A number of numerical example problems have been used to investigate in great detail these four ES-PIM models. Through these investigations, the

following conclusions can be drawn:

- All the four ES-PIM models can pass the standard patch test. Thus, they are linearly conforming and the numerical solutions of ES-PIMs are guaranteed to converge to the exact solution, despite the use of discontinuous PIM shape functions.
- In terms of the displacement error, the ES-PIMs obtain a similar or higher convergence rate compared to the FEM and NS-PIM(T3), which depends on the problem. In terms of accuracy, all the four ES-PIM models obtain better accuracy, about-ten-times-more-accurate solutions than for the FEM.
- In terms of the energy error, all the four ES-PIM models can obtain much better accuracy and a higher convergence rate than the linear FEM. Depending on the problem, the convergence rate of the ES-PIM may be a little higher even than the theoretical value of 1.5 for the W^2 formulation.
- In terms of efficiency, all the ES-PIM models are more efficient than the FEM with respect to both the errors in displacement and energy norms.
- The ES-RPIM (T6) and ES-RPIM (T2L) models obtain similar results in terms of accuracy and convergence rate, although the latter uses more nodes for interpolation. Generally, the T6 scheme achieves similar or higher efficiency than the T2L scheme and thus the former is preferred for practical computing.
- The four ES-PIM models perform more softly than the FEM and more stiffly than the NS-PIM(T3), and hence the computed strain energies of the ES-PIM are bounded by the FEM and NS-PIM(T3) from lower and upper.
- As to using quadratic interpolation for interior cells, the ES-PIM of the T6/3 scheme performs even more softly than the ES-PIM of the T3 scheme when the problem domain is discretized with “more” background cells.
- The ES-RPIM(T2L) uses more nodes for interpolation than the ES-RPIM(T6), and hence the former performs more softly than the latter.

References

- Chen, J. S., Wu, C. T., Yoon, S. and You, Y. [2001] A stabilized conforming nodal integration for Galerkin mesh-free methods, *Int. J. Numer. Meth. Eng.* **50**, 435–466.
- Dai, K. Y., Liu, G. R. and Nguyen, T. T. [2007] An n -sided polygonal smoothed finite element method (nSFEM) for solid mechanics, *Finite Elements in Analysis and Design*, **43**, 847–860.
- Kee, B. B. T., Liu, G. T., Song, C. X., Zhang, J. and Zhang, G. Y. [2007] A study on the effect of the number of local nodes for meshfree methods based on radial basis functions, *SIAM J. Numer. Anal.* (revised).
- Li, Y., Liu, G. R., Luan, M. T., Dai, K. Y., Zhong, Z. H., Li, G. Y. and Han, X. [2007] Contact analysis for solids based on linearly conforming radial point interpolation method, *Comput. Mech.* **39**, 537–554.
- Liu, G. R. [2002] *Meshfree Methods: Moving Beyond the Finite Element Method* (CRC, Boca Raton).

- Liu, G. R. [2008a] A generalized gradient smoothing technique and the smoothed bilinear form for Galerkin formulation of a wide class of computational methods, *Int. J. Comput. Meth.* **5**(2), 199–236.
- Liu, G. R. [2008b] A weakened weak (W^2) form for a unified formulation of compatible and incompatible displacement methods, *Int. J. Numer. Meth. Eng.* (revised).
- Liu, G. R. and Gu, Y. T. [2001] A point interpolation method for two-dimensional solids, *Inter. J. Numer. Meth. Eng.* **50**, 937–951.
- Liu, G. R. and Gu, Y. T. [2005] *An Introduction to Meshfree Methods and Their Programming* (Springer, Dordrecht).
- Liu, G. R., Nguyen, T. T. and Lam, K. Y. [2008] An edge-based smoothed finite element method (ES-FEM) for static and dynamic problems of solid mechanics, *J. Sound Vib.* (pub. online: DOI:10.1016/j.jsv.2008.08.027).
- Liu, G. R. and Quek, S. S. [2003] *Finite Element Method: A Practical Course* (Butterworth–Heinemann, Burlington).
- Liu, G. R., Dai, K. Y. and Nguyen T. T. [2007] A smoothed finite element method for mechanics problems, *Comput. Mech.* **39**, 859–877.
- Liu, G. R., Nguyen, T. T., Nguyen, X. H. and Lam, K. Y. [2007a] A node-based smoothed finite element method (NS-FEM) for upper bound solutions to solid mechanics problems, *Comput. Struct.* (pub. online: DOI:10.1016/j.compstruc.2008.09.003).
- Liu, G. R., Zhang, G. Y., Dai, K. Y., Wang, Y. Y., Zhong, Z. H., Li, G. Y. and Han, X. [2005] A linearly conforming point interpolation method (LC-PIM) for 2D mechanics problems, *Int. J. Comput. Meth.* **2**(4), 645–665.
- Liu, G. R. and Zhang, G. Y. [2008] Upper bound solution to elasticity problems: A unique property of the linearly conforming point interpolation method (LC-PIM), *Int. J. Numer. Meth. Eng.* **74**, 1128–1161.
- Liu, G. R., Li, Y., Dai, K. Y., Luan, M. T. and Xue, W. [2006] A linearly conforming radial point interpolation method for solid mechanics problems, *Int. J. Comput. Meth.* **3**, 401–428.
- Liu, G. R., Nguyen, T. T., Dai, K. Y. and Lam, K. Y. [2007b] Theoretical aspects of the smoothed finite element method (SFEM), *Int. J. Numer. Meth. Eng.* **71**, 902–930.
- Nguyen, T. T., Liu, G. R., Lam, K. Y. and Zhang, G. Y. [2008] A face-based smoothed finite element method (FS-FEM) for 3D linear and nonlinear solid mechanics problems using 4-node tetrahedral elements, *Int. J. Numer. Meth. Eng.* (pub. online: DOI: 10.1002/nme.2491).
- Pian, T. H. H. and Wu, C. C. [2006] *Hybrid and Incompatible Finite Element Methods* (CRC, Boca Raton).
- Powell, M. J. D. [1992] The theory of radial basis function approximation in 1990, in *Advances in Numerical Analysis*, ed. Light, F. W. (Oxford University Press), pp. 303–322.
- Simo, J. C. and Rifai, M. S. [1990] A class of mixed assumed strain methods and the method of incompatible modes, *Int. J. Numer. Meth. Eng.* **29**, 1595–1638.
- Timoshenko, S. P. and Goodier, J. N. [1970] *Theory of Elasticity*, 3rd edn. (McGraw-Hill, New York).
- Wang, J. G. and Liu, G. R. [2002] A point interpolation meshless method based on radial basis functions, *Int. J. Numer. Meth. Eng.* **54**, 1623–1648.
- Zhang, G. Y., Liu, G. R. and Li, Y. [2008] An efficient adaptive analysis procedure for certified solutions with exact bounds of strain energy for elasticity problems, *Finite Elements in Analysis and Design* **44**, 831–841.

- Zhang, G. Y., Liu, G. R., Nguyen, T. T., Song, C. X., Han, X., Zhong, Z. H. and Li, G. Y. [2007a] The upper bound property for solid mechanics of the linearly conforming radial point interpolation method (LC-RPIM), *Int. J. Comput. Meth.* **4**(3), 521–541.
- Zhang, G. Y., Liu, G. R., Wang, Y. Y., Huang, H. T., Zhong, Z. H., Li, G. Y. and Han, X. [2007b] A linearly conforming point interpolation method (LC-PIM) for three-dimensional elasticity problems, *Int. J. Numer. Meth. Eng.* **72**, 1524–1543.
- Zienkiewicz, O. C. and Taylor, R. L. [2000] *The Finite Element Method*, 5th edn. (Butterworth–Heinemann, Oxford).